slot width s increases. The sharp peak may again be greater than the broad peak as indicated by the case of $s = 1.00$ mm. Again the effective dielectric constant is not strongly dependent on the slot width.

One conclusion from Fig. 3 to Fig. 5 is that the thickness of the substrate is the most important parameter in affecting the leakage attenuation. The effect of changing slot width is somewhat higher than that of the changing strip width, but both are minor in comparsion with that of substrate thickness.

V. Conclusions

The dispersion and leakage characteristics such as the effective dielectric constant and normalized attenuation constant of coplanar waveguide have been treated using the spectral-domain approach together with the complex residue technique. To handle the complex propagation constant of the coplanar waveguide, the Fourier transform and the Parseval's theorem in complex plane are properly extended. A number of numerical results, such as the effective dielectric constant and normalized attenuation constant, have been presented to illustrate the characteristics of coplanar waveguide. Sharp peaks just after leakage together with broad peaks are two interesting phenomena observed in the attenuation characteristics. The physical mechanism of these peaks and the detail of transition in ϵ_{eff} and α/k_0 curves are still unclear and are worthy of further study.

References

[1] C. P. Wen, "Coplanar waveguide: a surface strip transmission line suitable for nonreciprocal gyromagnetic device application," *IEEE Trans. Microwave Theory Tech.*, vol. MTT-17, pp. 1087–1090, Dec. 1969.

[2] R. W. Jackson, "Considerations in the use of coplanar waveguide for millimeterwave integrated circuits," *IEEE Trans. Microwave Theory Tech.*, vol. MTT-34, pp. 1450–1456, Dec. 1986.

[3] C. N. Chang, Y. C. Wong, and C. H. Chen, "Full-wave analysis of coplanar waveguides by variational conformal mapping technique," *IEEE Trans. Microwave Theory Tech.*, vol. 38, pp. 1339–1344, Sept. 1990.

[4] D. B. Rutledge, D. P. Neikirk, and D. P. Kasilingam, "Integrated circuit antennas," in *Infrared and Millimeter Waves*, vol. 10. New York: Academic Press, 1983.

[5] M. Riaziat, R. Majidi-Ahy, and I. J. Feng, "Propagation modes and dispersion characteristics of coplanar waveguides," *IEEE Trans. Microwave Theory Tech.*, vol. 38, pp. 245–251, Mar. 1990.

[6] D. S. Phatak and A. P. Defonzo, "Dispersion characteristics of optically excited coplanar striplines: pulse propagation," *IEEE Trans. Microwave Theory Tech*, vol. 38, pp. 654–661, May 1990.

[7] H. Shigesawa, M. Tsuji, and A. A. Oliner, "Conductor backed slot line and coplanar waveguide: Dangers and full wave analysis," in *IEEE MTT-S Int. Microwave Symp. Dig.*, 1988, pp. 199–202.

[8] T. Rozzi, F. Moglie, E. Marchionna, and M. Politi, "Hybrid modes, substrate leakage, and losses of slotline at millimeter-wave frequencies," *IEEE Trans. Microwave Theory Tech.*, vol. 38, pp. 1069–1078, Aug. 1990.

[9] M. Tsuji, H. Shigesawa, and A. A. Oliner, "Printed-circuit waveguides with anisotropic substrates: A new leakage effect," in *IEEE MTT-S Int. Microwave Symp. Dig.*, 1989, pp. 783–786

[10] M. Tsuji, H. Shigesawa, and A. A. Oliner, "New interesting leakage behavior on coplanar waveguides of finite and infinite widths," *IEEE Trans. Microwave Theory Tech.*, vol. 39, no 12, pp. 2130–2137, Dec. 1991.

[11] N. K. Das and D. M. Pozar, "A generalized spectral-domain Green's function for multilayer dielectric substrates with application to multilayer transmission lines," *IEEE Trans. Microwave Theory Tech.*, vol. MTT-35, pp. 326–335, Mar. 1987.

[12] K Uchida, T. Noda, and T. Matsunaga, "New type of spectral-domain analysis of a microstrip line," *IEEE Trans. Microwave Theory Tech*, vol. 37, pp. 947–952, June 1989.

[13] D. S. Phatak, N. K. Das, and A. P. Defonzo, "Dispersion characteristics of optically excited coplanar striplines: comprehensive full-wave analysis," *IEEE Trans. Microwave Theory Tech.*, vol. 38, pp. 1719–1730, Nov. 1990.

[14] N. K. Das and D. M. Pozar, "Full-wave spectral-domain computation of material, radiation, and guided wave losses in infinite multilayered printed transmission lines," *IEEE Trans. Microwave Theory Tech.*, vol. 39, pp. 54–63, Jan. 1991.

The Scattering Matrix Formulation for Overmoded Coaxial Cavities

W. Lawson and P. E. Latham

***Abstract*—The scattering matrix formulation for complex right-circular cavities is extended to coaxial circuits with variable inner radii. The modified eigenvectors, which include the TEM wave, and the modified boundary conditions are presented. The properties of several configurations are examined and transmission measurements are shown to be in good agreement with theory.**

I. Introduction

The operation of coaxial transmission lines in frequency bands where only the TEM mode can propagate is straightforward and widespread. However, some potential applications, including high power microwave tubes, require highly overmoded coaxial circuits. Gyrotrons, for example, have utilized coaxial circuits operating in the $TE_{5,2}$ mode [1], and more recently in the $TE_{20,13}$ mode [2]. The principle advantage of coaxial cavities over right circular cavities is the enhancement in stable operation due to the decrease in mode density.

This work describes the calculation of resonant frequencies (real part and diffractive quality factor) for overmoded coaxial cavities. It is an extension of previous results which utilize the scattering matrix approach [3]–[7] to analyze right circular cavities [8]. The addition of the inner conductor results in four complications. First, coaxial systems can support TEM waves. Second, the radial dependence of the fields involve bessel functions of the second kind. A consequence of the second fact is that the perpendicular wave number becomes a complicated function of the inner and outer radii. Finally, variations in the radius of the inner conductor result in additional boundary conditions.

In Section II, the analysis is described briefly and the coefficients of the mode coupling matrix are presented. Typical numerical results, along with some experimental data, are described in Section III. The final section summarizes the results of this work.

II. Theory

Because the scattering matrix approach is described in detail elsewhere [8], only a brief outline is given here. In this approach, a cavity is divided into regions with uniform cross section and the

Manuscript received November 1, 1991; revised March 12, 1992. This work was supported by the U.S. Department of Energy.

The authors are with the Laboratoyr for Plasma Research, University of Maryland, College Park, MD 20742.

IEEE Log Number 9202145.

electromagnetic fields in each region are expanded in terms of the eigenmodes in that region. The expansion coefficients are determined by matching boundary conditions at the discontinuities between regions. This process is facilitated by computing the Mode Coupling (MC) matrices, whose elements are generated by expressing the eigenmodes in one region in terms of the eigenmodes in the adjacent region and can be expressed as

$$P_{mi}^{k} = \int d^2x_\perp \vec{e}_m^{\,k} \cdot (\vec{e}_i^{\,k+1})^*. \tag{1}$$

The integral is over the common cross-sectional area, $\vec{e}_m$ is the mth normalized tangential electric field, and the superscript refers to the boundary number. The MC matrices are coupled by the scattering process with matrices which represent the propagation of the electromagnetic waves in the constant cross-section waveguide sections. We follow exactly the notation in [8]; expressions for the full set of fields and the final cascaded matrix are given there. The differences between the coaxial and right circular cavities manifest themselves mainly in the coefficients of the (frequency-independent) MC matrix. These coefficients have already been computed for right circular cavities; here we compute them for coaxial systems.

Fig. 1 shows the junction between two perfectly conducting waveguides with different inner and outer radii. Without loss of generality, assume that the boundary of Region 2 is contained entirely with Region 1, i.e., $r_{o2} \le r_{o1}$ and $r_{i2} \ge r_{i1}$. The case of Region 1 being contained entirely with Region 2 can be handled with a simple matrix transposition. The mixed boundary case, when $r_{o2} > r_{o1}$ and $r_{i2} > r_{i1}$ or when $r_{o2} < r_{o1}$ and $r_{i2} < r_{i1}$, can be handled by adding a zero length region which yields two unmixed boundaries [8].

The eigenmodes in coaxial geometry depend on the cross-products of bessel functions, which are defined below:

$$p_n(x, y) = J_n(x)Y_n(y) - J_n(y)Y_n(x)$$

$$q_n(x, y) = J_n(x)Y_n'(y) - J_n'(y)Y_n(x)$$

$$r_n(x, y) = J_n'(x)Y_n(y) - J_n(y)Y_n'(x)$$

$$s_n(x, y) = J_n'(x)Y_n'(y) - J_n'(y)Y_n'(x)$$

where J_n and Y_n are bessel functions of the first and second kind, respectively. For TM modes, the pth eigenfunction for the nth azimuthal mode is (in cylindrical coordinates):

$$T_{np}^{M} = k_{np}^{M} p_n(\gamma_{np}\rho, \gamma_{np}r_i) \exp(jn\phi) \tag{2a}$$

where $j = \sqrt{-1}$. The normalization factor, k_{np}^{M}, is chosen to be

$$k_{np}^{M} = \{\pi[(\gamma_{np}r_o)^2 r_n^2(\gamma_{np}r_o, \gamma_{np}r_i) - (2/\pi)^2]\}^{-1/2} \tag{2b}$$

the perpendicular wavenumber satisfies $\gamma_{np} = x_{np}/r_o$, and x_{np} is the pth solution of $p_n(x_{np}, x_{np}r_i/r_o) = 0$. The normalized tangential electric field is given by $\vec{e}_{np} = \vec{\nabla}_t T_{np}^{M}$ where $\vec{\nabla}_t = \hat{\rho}(\partial/\partial\rho) + \hat{\phi}(jn/\rho)$. For TE modes, the eigenfunction is

$$T_{np}^{E} = k_{np}^{E} q_n(\gamma_{np}\rho, \gamma_{np}r_i) \exp(jn\phi). \tag{3a}$$

The normalization factor is

$$k_{np}^{E} = \left\{ \pi \left[((\gamma_{np}r_o)^2 - n^2) q_n^2(\gamma_{np}r_o, \gamma_{np}r_i) - ((\gamma_{np}r_i)^2 - n^2) \left(\frac{2}{\pi\gamma_{np}r_i} \right)^2 \right] \right\}^{-1/2}, \tag{3b}$$

where $\gamma_{np} = y_{np}/r_o$, and y_{np} is the pth solution of $s_n(y_{np}, y_{np}r_i/r_o) = 0$. The normalized tangential electric field is given by $\vec{e}_{np} = -\hat{z} \times \vec{\nabla}_t T_{np}^{E}$.

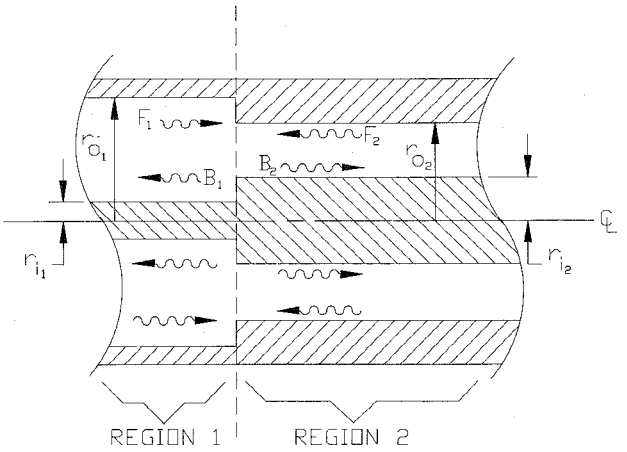

Fig. 1. Schematic of a boundary between two coaxial waveguides.

For the TEM mode, the eigenfunction is ($n = 0$):

$$T^{\mathrm{EM}} = k^{\mathrm{EM}} \ln(\rho) \tag{4a}$$

where

$$k^{\mathrm{EM}} = [2\pi \ln(r_o/r_i)]^{-1/2} \tag{4b}$$

The tangential electric field is $\vec{e} = \hat{\rho}k^{\mathrm{EM}}/\rho$. These definitions result in the condition

$$\int_0^{2\pi} d\phi \int_{r_i}^{r_o} \rho \, d\rho \, \vec{e}_{np} \cdot \vec{e}_{n'p'}^{\,*} = \delta_{nn'} \cdot \delta_{pp'}$$

where δ is the kroniker delta.

In principle, there are nine different cases for the elements of the MC matrix, depending on whether $\vec{e}_m^{\,1}$ and $\vec{e}_i^{\,2}$ are derived from the TE, TM, or TEM modes. However, four of the possibilities yield zero results because TE modes never couple to the TEM mode and TM modes in Region 2 (the smaller region) don't couple to either TEM or TE modes in Region 1. The remaining MC matrix components are found by integrating (1) either directly or by parts. The integration in the radial direction is from r_{i2} to r_{02}. The results are summarized below:

TE → TE:

$$P_{mi} = \frac{2\pi\gamma_i^2\gamma_m r_{o2} k_m^E k_i^E}{\gamma_i^2 - \gamma_m^2} \left[s_n(\gamma_m r_{o2}, \gamma_m r_{i1}) q_n(\gamma_i r_{o2}, \gamma_i r_{i2}) - \frac{2}{\pi} \left(\frac{1}{r_{o2}\gamma_i} \right) s_n(\gamma_m r_{i2}, \gamma_m r_{i1}) \right] \tag{5a}$$

TM → TM:

$$P_{mi} = \frac{2\pi\gamma_m^2\gamma_i r_{o2} k_m^M k_i^M}{\gamma_m^2 - \gamma_i^2} \left[r_n(\gamma_i r_{o2}, \gamma_i r_{i2}) p_n(\gamma_m r_{o2}, \gamma_m r_{i1}) + \frac{2}{\pi} \left(\frac{1}{r_{o2}\gamma_i} \right) p_n(\gamma_m r_{i2}, \gamma_m r_{i1}) \right] \tag{5b}$$

TM → TE:

$$P_{mi} = -2\pi jnk_i^E k_m^M \left[q_n(\gamma_i r_{o2}, \gamma_i r_{i2}) p_n(\gamma_m r_{o2}, \gamma_m r_{i1}) - \frac{2}{\pi} \left(\frac{1}{r_{i2}\gamma_i} \right) p_n(\gamma_m r_{i2}, \gamma_m r_{i1}) \right] \tag{5c}$$

TM → TEM:

$$P_{mi} = 2\pi k_m^M k_i^{\mathrm{EM}} [p_0(\gamma_m r_{o2}, \gamma_m r_{i1}) - p_0(\gamma_m r_{i2}, \gamma_m r_{i1})] \tag{5d}$$

TEM → TEM:

$$P_{mt} = 2\pi k_m^{EM} k_t^{EM} \ln (r_{o2}/r_{i2}). \quad (5e)$$

In (5), γ_m indicates γ_{nm} in Region 1 and γ_t indicates γ_{nt} in Region 2. It is straightforward to show that these matrix elements reduce to the ones given in [8] in the limit $r_{i1}, r_{i2} \to 0$.

III. Numerical Results

In this section we discuss two examples. First, the scattering formalism is used to calculate the resonant frequency of a cavity with a coupling aperture. Second, the approach is used to compute power transmission data through a coaxial circuit with a varying cross section.

Consider the microwave circuit shown in Fig. 2(a). The lengths and outer radii of the four regions are given in Table I. An inner conductor of variable radius, $0 \le r_i < 1.5$ cm, extends through the first three regions. A qualitative description of the dependence of resonant frequency on inner radius is as follows. First, assume $r_i = 0$ and consider all the closed cavity (CC) eigenfrequencies corresponding to the length and outer radius of region two. If an ideal (CC) resonant frequency is below the cutoff frequency of the lowest corresponding radial mode (usually the TE_{n1}) in the adjacent regions, then the eigenfrequency of the actual mode will be close to the CC frequency. Also, the corresponding quality factor (Q) will be quite high. Otherwise, the mode is a complicated "whole tube" mode whose energy is often not well localized.

Because the zeros of the TM modes, x_{np}, increase monotonically with inner radius (for a fixed outer radius), the corresponding TM eigenfrequencies and Qs increase with r_i. The cutoff frequencies of the TE_{n1} modes ($n > 0$) decrease, however, because y_{n1} approaches n as r_i approaches r_0. Therefore, the corresponding TE_{n1}, resonant frequencies and Qs decrease. The higher order $TE_{np}(p > 1)$ eigenfrequencies initially decrease, but then increase due to the interlacing of TE and TM mode zeros. The TE_{0n} cutoff frequencies are equal to the TM_{1n} frequencies, so the TE_{0n} resonant frequencies monotonically increase with inner radius.

For the circuit of Fig. 2(a), these concepts are illustrated in Fig. 3 with three representative modes. Fig. 3a represents the dependence of resonant frequency for modes with one axial variation when $r_i = 0$. The corresponding quality factors are shown in Fig. 3(b). The TE_{211} mode's resonant frequency is slightly below the CC result and decreases as predicted. The quality factor also decreases as predicted. The increase in both frequency and Q at the very end as $r_i \to r_o$ occurs because of the increased reflection at the predominantly metal boundary. The TE_{011} mode tracks the CC result almost exactly because of the large Q factor which quickly goes off the theoretical scale.

The behavior of the TM_{01} mode is considerably more complicated. When $r_i = 0$, the TM mode is moderately well cutoff, which results in a high Q (~ 400) and a resonant frequency near the CC result. The addition of an inner conductor allows coupling to the TEM (with no cutoff frequency) and drastically drops the Q. While the $r_i = 0$ limit is recovered, the quality factor drops to about $Q \sim 100$ when $r_i = 10^{-30}$ cm. The second complication involves mode crossings between the TEM and TM modes. The second axial TEM mode has a CC resonant frequency at 7.49 GHz. This results in the peak in Q and the slow variation in resonant frequency near $r_i = 0.7$ cm.

Fig. 2(b) shows the axial field variation in E_ϕ for the TE_{01} and TE_{21} modes at a radius of 1 cm when $r_i = 0.5$ cm. The figure reveals the continuity of E_ϕ at the boundaries. The relative peak is higher for the TE_{011} mode because of its higher Q. Likewise, the amplitude of the travelling wave ($t > 5.5$ cm) is larger for the

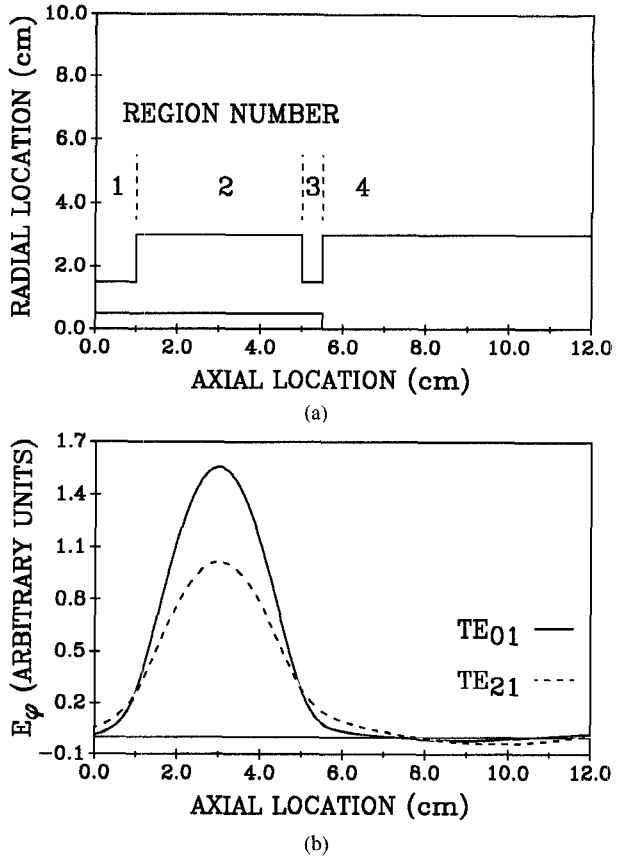

Fig. 2. (a) The simulated coaxial geometry. The inner radius is varied from zero to 1.49 cm. (b) The azimuthal field at $\rho = 1$ vs. axial distance for the TE_{01} and TE_{21} modes.

TABLE I
Coaxial Cavity Dimensions Corresponding to Fig. 2(a). (All Dimensions are in Centimeters)

Region #	1	2	3	4
Inner radius	r_i	r_i	r_i	0
Outer radius	1.5	3.0	1.5	3.0
Length	1.0	4.0	0.5	6.5

TE_{211} mode. Both fields exhibit an exponential decay for $z < 1$ cm.

Fig. 4 illustrates the continuity of transverse field for the TM mode at the boundary between regions 3 and 4. The inner radius is again fixed at 0.5 cm. Twenty-two modes were used in region 4. This is far more than required to get convergence in frequency, but still leaves some discrepancy in E_ρ due to the sharp discontinuities at the metal surfaces. The agreement in B_ϕ is nearly perfect. The large amplitude in B_ϕ to the right of the boundary indicates that considerable energy propagates out the right side.

For the second example, scattering matrix transmission calculations are compared with experimental measurements. Two coaxial circuits were built, and the comparison with TE_{11} transmission data is shown in Fig. 5. The signal is injected and extracted in standard X-band waveguide and two TE_{10} rectangular to TE_{11} circular waveguide adapters provide the required mode. Both circuits utilize a constant outer radius of 1.5 cm. For Fig. 5(a), the coaxial insert has $r_i = 0.5$ cm, has a length of 7.48 cm and has abrupt transitions to $r_i = 0$ at both ends. For Fig. 5(b), the coaxial insert has the same overall length and maximum radius, but has 31° lin-

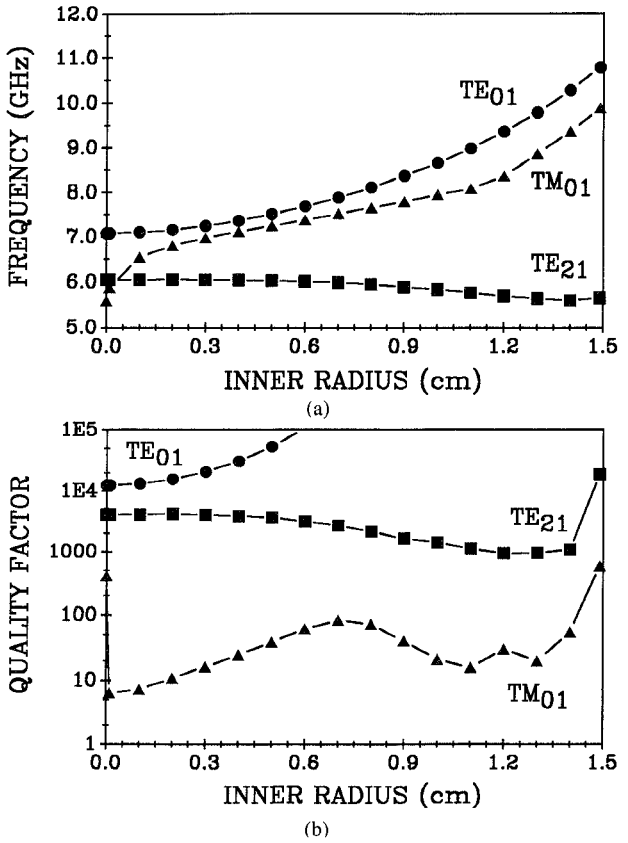

Fig. 3. (a) The frequency dependence of the TE_{011}, TM_{011}, and TE_{211} modes on inner radius. (b) The dependence of quality factor on inner radius.

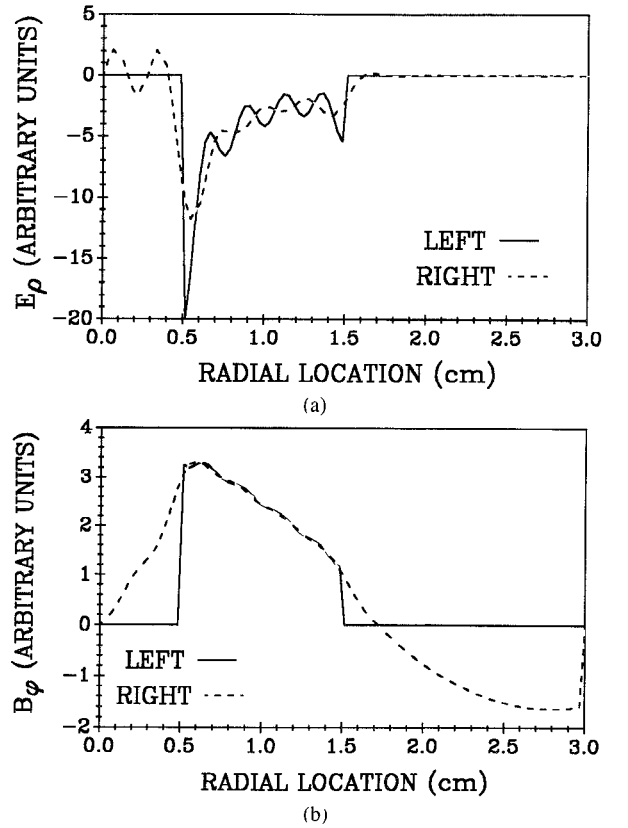

Fig. 4. Evaluation of the boundary conditions at the $z = 5.5$ cm interface (a) continuity of E_ρ and (b) continuity of B_ϕ.

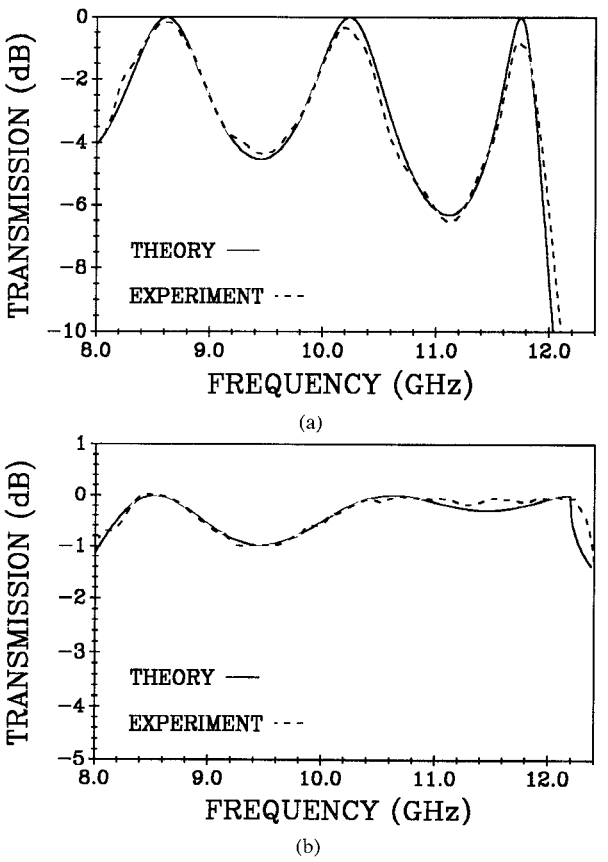

Fig. 5. A comparison of theoretical and experimental TE_{11} transmission data (a) for a simple coaxial insert and (b) for a tapered coaxial insert.

ear tapers on both ends to make a smooth transition to the $r_i = 0$ regions. Each taper is modeled with ten regions that have appropriate inner radii. Agreement in both cases is good. The tapered case has much better transmission properties as expected. Above 12.2 GHz, the TM_{11} mode can propagate in the $r_i = 0$ regions but are reflected by the mode converters. This effect results in the slight discrepancies at the upper frequency points.

IV. Summary

The scattering matrix formulation of right circular cavities has been extended to overmoded coaxial cavities. The TEM mode is included for proper evaluation of TM_{0n} modes. The code converges rapidly and can simulate both abrupt discontinuities and smooth changes in the inner and outer radii. Experimental transmission data agrees well with theory.

Acknowledgment

The authors would like to acknowledge useful discussions with B. Hogan and C. D. Striffler.

References

[1] Yu. V. Bykov, A. L. Gol'denberg, L. V. Nikolaev, M. M. Ofitserov, and M. I. Petelin, "Experimental investigation of a gyrotron with whispering-galley modes," *Izvestiya Vysshikh Uchebnykh Zavedenii, Radiofizika*, vol. 18, p. 1544, 1975.

[2] A. L. Gol'denberg, A. B. Pavelyev, and V. I. Khizhuyak, in *Gyrotrons: Book of Collected Papers*, V. A. Flyagin, Ed., Gorky, USSR: IAP, 1989, p. 20 (in Russian).

[3] A. Wexler, "Solution of waveguide discontinuities by modal analysis," *IEEE Trans. Microwave Theory Tech.*, vol. MTT-15, p. 508, 1967.

[4] F. Sporleder and H. G. Unger, *Waveguide Tapers, Transitions, and Couplers*. New York: Peregrinus, 1974.
[5] G. L. James, "Analysis and design of TE_{11}-to-HE_{11} corrugated waveguide mode converters," *IEEE Trans. Microwave Theory Tech.* vol. MTT-29, p. 1059, 1981.
[6] H. Patzelt and F. Arndt, "Double-plane steps in rectangular waveguides and their application to transformers, irises, and filters," *IEEE Trans. Microwave Theory Tech.* vol. MTT-30, p. 771, 1982.
[7] H. Auda and R. F. Harrington, "A moment solution for waveguide junction problems," *IEEE Trans. Microwave Theory Tech.*, vol. MTT-32, p. 515, 1983.
[8] J. M. Neilson, P. E. Latham, M. Caplan, and W. Lawson, "Determination of the resonant frequencies in a complex cavity using the scattering matrix formulation," *IEEE Trans. Microwave Theory Tech.*, vol. 37, p. 1165, 1989.

Method of Interpolation Factorization (MIF) for the Solution of Two-Dimensional Diffraction Problems

Vladimir Volman and Jacques Gavan

***Abstract*—A new method for exact solution of two-dimensional diffraction problems is presented.**

I. Introduction

One of the effective numerical-analytical methods for the solution of a wide class of diffraction problems is the modified method of residues [1], [2]. The principal difficulties in this method appear when we begin the construction of a meromorphic function. Let's consider a new method for the solution of this problem. For clearness we shall consider TEM-analysis of a strip line (Fig. 1). As shown in [2], this problem leads to the construction of a meromorphic function $F(\omega)$, which satisfies the following conditions:

1) $F(\omega)$ has simple poles for $\omega = \alpha_{n1}$, where $n = 1, 2, \cdots, \infty$, and for $\omega = 0$;
2) $F(\alpha_{nj}) + \lambda_{nj}F(-\alpha_{nj}) = 0$, for $n = 1, 2, \cdots, \infty, j = 2, 3$; λ_{nj} and α_{nj} are known values [2].
3) $F(\omega)$ has the asymptotic behavior $|\omega \angle^{-3/2}$ for $|\omega| = \infty$;
4) the residue of $F(\omega)$ for $\omega = 0$ is equal to (-1),

II. Presentation of the Problem

Let's introduce a function similar to those described in [2]

$$F(\omega) = -\frac{\exp(\nu\omega)}{\omega}\prod_{n=1}^{\infty}\frac{(1-\omega/\alpha'_{n2})(1-\omega/\alpha'_{n3})}{(1-\omega/\alpha_{n1})},$$

$$\nu = [a_3 \ln(a_1/a_3) + a_2 \ln(a_1/a_2)]/\pi, \tag{1}$$

where α'_{n2} and α'_{n3} are unknown zeros of $F(\omega)$.

$F(\omega)$ satisfies in such form the 4th condition and fulfill the asymptotic behavior $|\omega|^{-3/2}$ for the following conditions [2]:

$$\alpha'_{nj} = n\pi/a_j, \qquad n \to \infty \text{ and } j = 2, 3, \tag{2}$$

Manuscript received April 29, 1991; revised February 10, 1992.

V. Volman is with The Hebrew University of Jerusalem, The Rechah Institute of Physics, Givat Ram, 91904 Jerusalem, Israel.
J. Gavan is with the Center for Technological Education Holon, P.O.B. 305, Holon 58102, Israel.

IEEE Log Number 9202146.

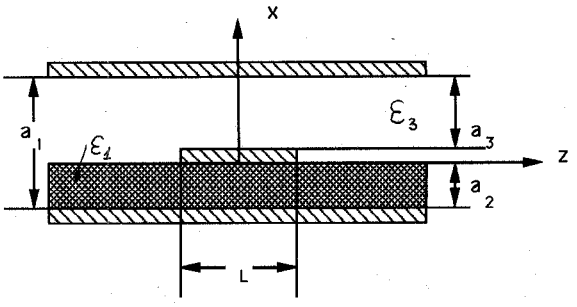

Fig. 1. View of strip line.

where a_j are known constants [2] and $a_1 = a_2 + a_3$. Therefore,

$$F(\omega) = -\frac{\exp(\nu\omega)}{\omega}R_{3M}(\omega)\prod_{n=M+1}^{\infty}\frac{(1-\omega a_2/n\pi)(1-\omega a_3/n\pi)}{(1-\omega a_1/n\pi)}, \tag{3}$$

where

$$R_{3M}(\omega) = \prod_{n=1}^{M}\frac{(1-\omega/\alpha'_{n2})(1-\omega/\alpha'_{n3})}{(1-\omega/\alpha_{n1})}, \tag{4}$$

and M is a number from which the asymptotic value presented in (2) may be used. Let us introduce the rational fractional function

$$G_0(\omega) = \frac{R_{3M}(\omega)}{R_{3M}(-\omega)}\bigg|_{\omega=\alpha_m} = \prod_{n=1}^{M} \cdot \frac{(1+\omega/\alpha_{n1})(1-\omega/\alpha'_{n2})(1-\omega_3\alpha'_{n3})}{(1-\omega/\alpha_{n1})(1+\omega/\alpha'_{n2})(1+\omega/\alpha_{n3})}\bigg|_{\omega=\alpha_m}$$

$$= \{\lambda_m^{(0)}\}_1^{3M},$$

$$\{\alpha_m\}_1^{3M} = \{-\alpha_{m1}, \alpha_{m2}, \alpha_{m3},\}_1^M, \{\lambda_m^{(0)}\}_1^{3M}$$

$$= \{0, \lambda_{m2}, \lambda_{m3}\}_1^M \tag{5}$$

It is evident that

$$G_0(-\omega) = 1/G_0(\omega). \tag{6}$$

Let U_ω be the class of rational fractional functions satisfying (6). Then the considering problem leads to an interpolation problem in order to define the function $G_0(\omega)$ from the class U_ω, which is equal to

$$G_0(\alpha_m\} = \{\lambda_m^{(0)}\}_1^{3M} \tag{7}$$

III. Build Up of the Function $F(\omega)$

Consider the rational fractional function of class U_ω

$$G_0(\omega) = \frac{(\alpha_1-\omega)G_1(\omega) + (\alpha_1+\omega)G_0(\alpha_1)}{(\alpha_1+\omega) + (\alpha_1-\omega)G_0(\alpha_1)G_1(\omega)} \tag{8}$$

where $G_1(\omega) \in U_\omega$ and at the point $\omega = \alpha_1 G_0(\alpha_1)$ is equal to λ_1 independently of the selection of $G_1(\omega)$.

The values $G_1(\omega)$ are chosen at the points $\alpha_m (3M \geqslant m \geqslant 2)$ so that the (7) is satisfied not only at the point α_1 but at all the points $\alpha_m (m \geqslant 2)$. According to (8)

$$G_1(\alpha_m) = \frac{(\lambda_m^{(0)} - \lambda_1^{(0)})(\alpha_1+\alpha_m)}{(1-\lambda_m^{(0)}\lambda_1^{(0)})(\alpha_1-\alpha_m)} = \{\lambda_m^{(1)}\}_2^M. \tag{9}$$